Journal of Pathology
J Pathol June 2024; **263:** 242–256
Published online 5 April 2024 in Wiley Online Library
(wileyonlinelibrary.com) DOI: 10.1002/path.6280

ORIGINAL ARTICLE

Co-targeting BET, CBP, and p300 inhibits neuroendocrine signalling in androgen receptor-null prostate cancer

Nicholas Choo[1], Shivakumar Keerthikumar[1,2,3], Susanne Ramm[3,4], Daisaku Ashikari[1†], Linda Teng[1], Birunthi Niranjan[1], Shelley Hedwards[1], Laura H Porter[1], David L Goode[2,3,5], Kaylene J Simpson[3,4,6], Renea A Taylor[2,3,7,8], Gail P Risbridger[1,2,3,8] and Mitchell G Lawrence[1,2,3,8*]

[1] *Department of Anatomy and Developmental Biology, Biomedicine Discovery Institute Cancer Program, Monash University, Clayton, Victoria, Australia*
[2] *Peter MacCallum Cancer Centre, Melbourne, Victoria, Australia*
[3] *Sir Peter MacCallum Department of Oncology, The University of Melbourne, Melbourne, Victoria, Australia*
[4] *Victorian Centre for Functional Genomics, Peter MacCallum Cancer Centre, Melbourne, Victoria, Australia*
[5] *Computational Cancer Biology Program, Peter MacCallum Cancer Centre, Melbourne, Victoria, Australia*
[6] *Department of Biochemistry and Pharmacology, The University of Melbourne, Parkville, Victoria, Australia*
[7] *Department of Physiology, Biomedicine Discovery Institute Cancer Program, Monash University, Clayton, Victoria, Australia*
[8] *Cabrini Institute, Cabrini Health, Malvern, Victoria, Australia*

**Correspondence to: MG Lawrence, Department of Anatomy and Developmental Biology, Biomedicine Discovery Institute Cancer Program, 19 Innovation Walk, Monash University, Clayton, VIC 3800, Australia. E-mail: mitchell.lawrence@monash.edu*

†*Present address:* Department of Urology, Nihon University School of Medicine, Tokyo, Japan

Abstract

There are diverse phenotypes of castration-resistant prostate cancer, including neuroendocrine disease, that vary in their sensitivity to drug treatment. The efficacy of BET and CBP/p300 inhibitors in prostate cancer is attributed, at least in part, to their ability to decrease androgen receptor (AR) signalling. However, the activity of BET and CBP/p300 inhibitors in prostate cancers that lack the AR is unclear. In this study, we showed that BRD4, CBP, and p300 were co-expressed in AR-positive and AR-null prostate cancer. A combined inhibitor of these three proteins, NEO2734, reduced the growth of both AR-positive and AR-null organoids, as measured by changes in viability, size, and composition. NEO2734 treatment caused consistent transcriptional downregulation of cell cycle pathways. In neuroendocrine models, NEO2734 treatment reduced *ASCL1* levels and other neuroendocrine markers, and reduced tumour growth *in vivo*. Collectively, these results show that epigenome-targeted inhibitors cause decreased growth and phenotype-dependent disruption of lineage regulators in neuroendocrine prostate cancer, warranting further development of compounds with this activity in the clinic.

Keywords: prostate cancer; neuroendocrine; organoids; PDX; NEO2734; BRD4; CBP/p300

Received 5 October 2023; Revised 30 January 2024; Accepted 29 February 2024

Conflict of interest statement: RAT, GPR, and MGL declare research collaborations (Pfizer, AstraZeneca). NEO2734 was supplied by Epigene Therapeutics. All other authors had no conflicts of interest to declare.

Introduction

Neuroendocrine prostate cancer (NEPC) is difficult to treat. As the androgen receptor (AR) is not expressed in these tumours, they are inherently resistant to androgen deprivation therapy and AR signalling inhibitors. NEPC is also heterogeneous, arising at different clinical stages and with varying histopathologies [1].

In rare cases, patients are diagnosed with NEPC [2]. More commonly, patients develop treatment-induced NEPC, which arises from AR-positive adenocarcinoma due to ongoing suppression of AR signalling [3,4]. The different types of NEPC include small cell and large cell tumours, which have different cytology, but both express neuroendocrine markers such as synaptophysin and chromogranin A. In addition to NEPC, some tumours are referred to as double-negative prostate cancer, because they lack the AR and neuroendocrine markers [4]. Herein, we collectively refer to NEPC and double-negative prostate cancer as AR-null.

The transition from adenocarcinoma to AR-null prostate cancer arises through permissive genomic alterations and epigenome remodelling. Deletions and loss-of-function mutations of *TP53*, *RB1*, and *PTEN* are enriched in AR-null prostate cancer [3,4]. In addition,

AR-null phenotypes are reinforced by lineage-associated transcription factors and chromatin remodelling factors, such as ASCL1, FOXA2, BRN2, and CARM1 [5–8]. Accordingly, AR-null prostate cancer has distinct patterns of DNA methylation and chromatin accessibility versus AR-positive adenocarcinoma [3,5,9]. These changes promote rapid proliferation and the expression of characteristic markers of NEPC.

As chromatin remodelling reinforces the phenotype of AR-null prostate cancer, there is interest in therapies that disrupt this process. Several compounds in preclinical development and clinical trials target proteins that either modify histones (e.g. CBP/p300, EZH2, HDACs, and LSD1) or recognise histone modifications (e.g. BRD4) [10]. This includes inhibitors of CBP/p300 and BET proteins, which have been investigated in a variety of malignancies, given that CBP/p300 and BET proteins are widely expressed across cell types [11,12].

CBP/p300 and BET inhibitors have also been examined in prostate cancer, but largely in the context of disrupting AR signalling. CBP, p300, and BRD4 expression levels have been correlated with AR expression and activity, but their relative expression in AR-null prostate cancer is unclear [13,14]. Moreover, initial preclinical studies with several CBP/p300 and BET inhibitors found them to be less effective in AR-null versus AR-positive prostate cancer [14–17]. As these observations were based on limited AR-null models, typically DU145 and PC3 cells, they may not accurately represent the overall activity of epigenome-targeting agents in AR-null prostate cancer.

More recent preclinical and clinical data, especially for BET inhibitors, support targeting chromatin remodelling in prostate cancer with low or no AR activity. Enzalutamide-resistant LNCaP sublines with AR-low, neuroendocrine-positive phenotypes were sensitive to BET inhibition, in part due to downstream disruption of E2F1 function [18]. BET inhibitors also decreased the viability of additional AR-null models [18,19]. Notably, a phase 1 trial of the BET inhibitor ZEN-3694 in combination with enzalutamide showed that the patients with the lowest AR activity in pretreatment biopsies had the greatest responses [20]. Thus, BET inhibitors, and potentially other agents targeting histone readers, writers or erasers, have more promising activity in tumours with AR-low or AR-null phenotypes than anticipated from the initial screens in cell lines. Yet, little is known about the effects on neuroendocrine tumours completely lacking AR expression.

These observations prompted us to investigate the response of NEPC to therapies targeting chromatin remodelling. We treated patient-derived models of AR-positive, double-negative, and NEPC with NEO2734, a first-in-class dual inhibitor of CBP/p300 and BET proteins (BRD2, BDR3, BRD4) [21] that is in phase 1 trials for castrate-resistant prostate cancer (CRPC) (NCT05488548). We show that NEO2734 decreases the viability of AR-null models and downregulates lineage-related transcription factors that maintain the neuroendocrine phenotype.

Materials and methods

Further details of all experiments are provided in Supplementary materials and methods.

Establishment and treatment of patient-derived xenografts (PDXs)

Written informed consent was obtained from participants according to institutional human ethics approval from Monash University (1636; 36762; 12287), the Peter MacCallum Cancer Centre (11/102), Cabrini Hospital (03-14-04-08), and Eastern Health (E55/1213). All animal care was in accordance with Monash University animal ethics approvals (MARP 2012/158, MARP 2014/085, MARP 22185, and MARP 28911). All PDXs were previously established by the Melbourne Urological Research Alliance (MURAL) [22–25] and grown in male NSG mice. PDXs of castrate-sensitive prostate cancer were grown in mice supplemented with 5-mm testosterone implants, whereas PDXs of CRPC were grown in castrated host mice, as previously described [26–32].

For *in vivo* drug treatments, PDXs were established subcutaneously. Experiments were performed using the one animal per model per treatment approach ($1 \times 1 \times 1$) (one graft/mouse) [33]. Mice were treated via gavage with vehicle control or NEO2734 for 5 days per week for 11 or 28 days.

Immunohistochemistry

Tumour samples used for immunohistochemistry were from the MURAL and Movember GAP1 tissue microarrays (TMA), and larger pieces of fixed PDX tissue [22,34,35]. Automated immunohistochemistry staining was performed using the Leica BOND-MAX™ automated system (Leica Biosystems, Wetzlar, Hessen, Germany). Antibody details and staining conditions are listed in supplementary material, Table S1.

Organoids and explants

Organoid cultures were established using both manual and automated methods. Manually seeded organoids were grown in Matrigel and metabolic activity was measured using PrestoBlue. For high-throughput assays, organoids were seeded robotically in Matrigel in 384-well plates. On the final day of treatment, organoids were stained with Hoechst 33342 and imaged with brightfield and fluorescent images. Cell viability was measured using the CellTitre-Glo (CTG) Luminescent Cell Viability Assay. Images were analysed using CellProfiler software (Cambridge, MA, USA).

For RNA-sequencing, organoids were treated for 24 h with vehicle control or 1 μM NEO2734, and explants were treated for 48 h at 37 °C with vehicle control or 1 μM JQ1, before being collected for RNA-sequencing.

RNA-sequencing and data analysis

Total RNA was isolated using the RNAqueous™-Micro Total RNA Isolation Kit (Invitrogen™, Waltham, MA, USA) with an in-built DNase-I treatment following the manufacturer's instruction. Total RNA was quantified using a Nanodrop ND-1000 spectrophotometer and checked for purity and integrity in a Bioanalyzer-2100 device (Agilent Technologies, Santa Clara, CA, USA). RNA-sequencing was performed at AGRF (https://www.agrf.org.au/).

Libraries were prepared using Lexogen 3' Quantseq sequenced using NextSeq HO with 75 bp single-end reads. Raw reads from the Fastq files were checked for quality using FastQC v0.11.6 and low-quality bases were trimmed using Cutadapt v2.1. Trimmed reads were aligned against the reference genome hg38 using STAR aligner v2.7.5b. To remove mouse reads, the reads were separately aligned to human hg38 and mouse mm39 reference genomes using STAR aligner. XenofilteR v1.6 was used to select human-specific reads, and counts matrix were generated using HTseq v0.11.2. DESeq2 was used for differential expression analysis. For gene set enrichment analysis (GSEA), all genes were ranked by log2 fold-change and checked for the enrichment of MsigDB50 cancer hallmarks pathways using thr fgsea R package. Volcano plots of differentially expressed genes were plotted using ggplot2 in R v4.2.0.

Statistical analyses

All statistical analyses were conducted using GraphPad Prism 9 (GraphPad Software Inc, San Diego, CA, USA), with statistical significance set at $p < 0.05$. All statistical tests were two-tailed and are listed in the corresponding figure legends. Data are shown as mean ± SEM.

Results

BRD4, CBP, and p300 are expressed in AR-null prostate cancer

Previous studies have evaluated BRD4, CBP, and p300 expression in patient cohorts of prostate cancer; however, there is typically an under-representation of AR-null prostate cancer. Therefore, we comprehensively mapped mRNA and protein levels of BRD4, CBP, and p300 in AR-null versus AR-positive disease. We evaluated expression profiles in 72 PDXs from MURAL, a diverse cohort of AR-positive and AR-null PDXs of prostate cancer [22]. The lack of human stroma in PDXs enabled us to specifically quantify expression profiles of prostate cancer epithelium without confounding contributions from other cell types. *BRD4*, *CBP*, and *p300* expression profiles had different correlations with *AR* mRNA levels, and AR and neuroendocrine signatures (Figure 1A; supplementary material, Figure S1). Nevertheless, the correlation coefficients were modest, indicating no stark difference in *BRD4*, *CBP*, and *p300* mRNA abundance between prostate cancer pathologies.

We also quantified nuclear staining of BRD4, CBP, and p300 using immunohistochemistry in PDX tissues from two independent cohorts: MURAL and 98 prostate cancer PDXs from the Movember GAP1 consortium [34,35]. We confirmed the specificity of the antibodies through siRNA knockdown of BRD4, CBP, and p300 in DU145 cells (see supplementary material, Figure S2). Staining intensity varied within individual PDXs, but all three proteins were detectable in every PDX with a wide staining distribution in both PDX cohorts (see supplementary material, Figures S3 and S4A). BRD4, CBP, and p300 H-scores were correlated with one another, but with a wide spread in relative expression of each protein across PDXs (see supplementary material, Figure S4B). Consistent with mRNA expression, there was considerable overlap in the distributions of each factor between AR-positive and AR-null tumours (Figure 1B–D), with the only significant difference being increased p300 staining in AR-positive PDXs in the Movember GAP1 cohort (Figure 1D). Thus, BRD4, CBP, and p300 are all expressed in both AR-positive and AR-null tumours, with a spectrum of staining within and between tumours.

To investigate whether androgen deprivation alters BRD4, CBP, and p300 levels, we analysed six CRPC PDXs from the MURAL cohort with matched tumours grown in testosterone-supplemented and castrated hosts (see supplementary material, Figure S4C). There was a significant increase in nuclear BRD4 ($p < 0.05$) and p300 ($p < 0.05$) staining in all PDXs grown in castrated mice, based on paired analyses, whereas there was no significant difference for CBP ($p = 0.26$).

Overall, the mRNA and protein analyses showed that BRD4, CBP, and p300 are co-expressed across AR-positive and AR-null tumours, albeit at varying levels. Therefore, we next examined their potential as therapeutic targets for diverse phenotypes of prostate cancer.

NEO2734 suppresses the growth of prostate cancer organoids

We investigated whether NEO2734, which targets all three proteins, inhibits the growth of prostate cancer cells with different phenotypes. We grew organoids from six PDXs, including castrate-sensitive primary adenocarcinoma (287R), primary (224R-Cx, 305R-Cx) and metastatic (435.1A-Cx) NEPC, and metastatic CRPC with AR-positive (201.1A-Cx) and double-negative (201.2A-Cx) phenotypes (Figure 2A). In these organoids, we observed similar trends in the relationship of *BRD4*, *CBP*, and *p300* mRNA expression to *AR* expression (see supplementary material, Figure S5A). We treated organoids with increasing doses of NEO2734 (100–5,000 nM), with 5,000 nM used as a high dose to confirm changes in organoid viability across multiple endpoints.

We used CTG to measure the viability of organoids based on ATP levels. The two most sensitive organoids,

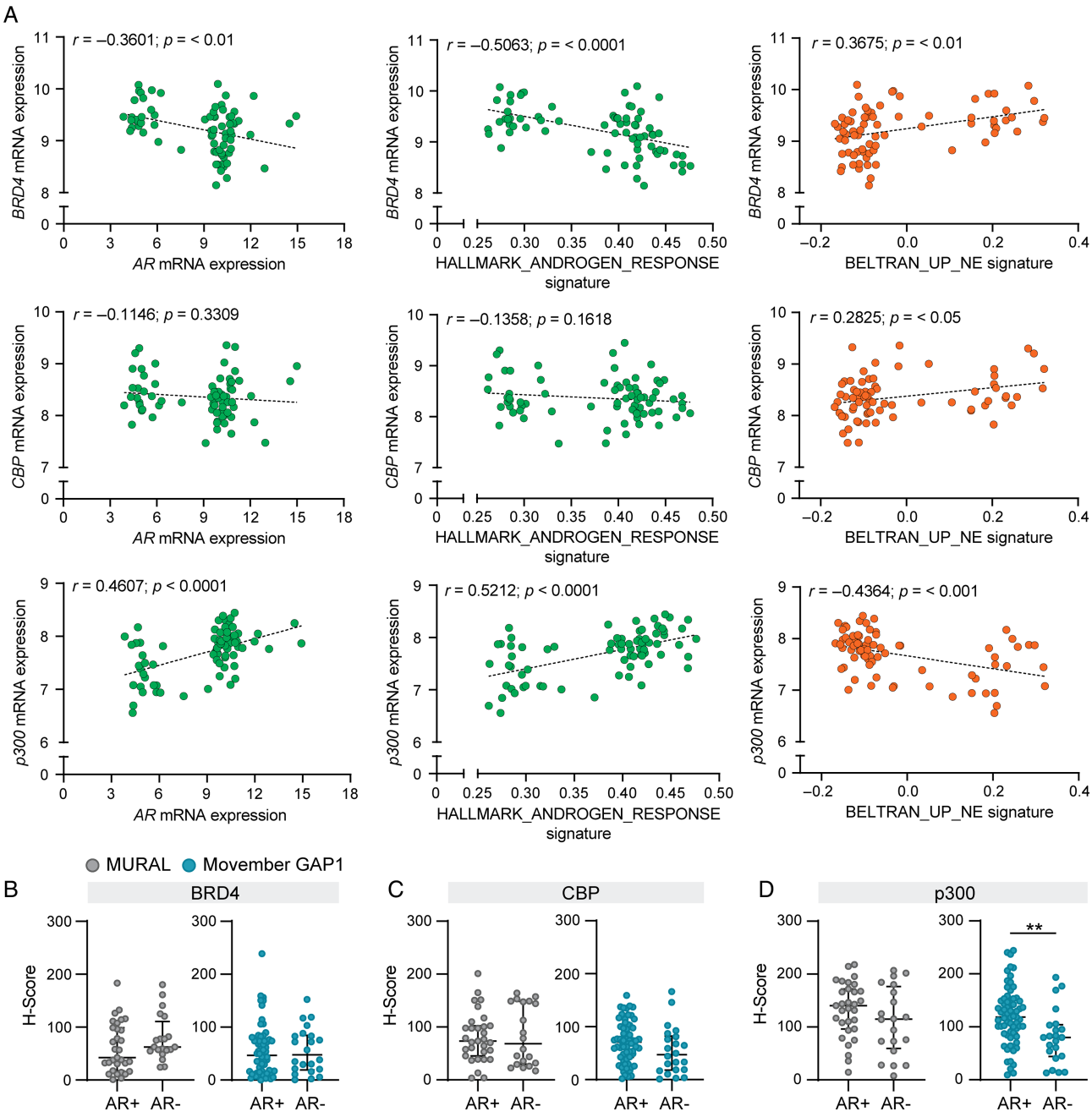

Figure 1. BRD4, CBP, and p300 are co-expressed in AR-positive and AR-null prostate cancer. (A) Correlation between *BRD4*, *CBP*, and *p300* (*EP300*) mRNA expression and the phenotype of 74 PDXs from the MURAL cohort. Plots show the correlation with AR mRNA expression and AR signature (HALLMARK_ANDROGEN_RESPONSE) (green) and neuroendocrine signature (BELTRAN_UP_NE) (orange). The *r*- and *p*-values were calculated using Pearson's correlations (*BRD4* and *CBP*) or Spearman's correlations (*p300*), depending on the distribution of the data. (B–D) Quantification of immunohistochemistry (H-scores) for (B) BRD4, (C) CBP, and (D) p300 in AR-positive and AR-null PDXs in the MURAL (grey) and Movember GAP1 (blue) cohorts (AR-positive, $n = 31$; AR-null, $n = 20$). The median H-score and interquartile range are shown. $^{**}p < 0.01$; unpaired *t*-test. NE, neuroendocrine.

201.1A-Cx (AR-positive) and 224R-Cx (AR-null), had significantly decreased viability at the lowest NEO2734 dose, with a low to moderate decrease in metabolic activity for the remaining four organoids (Figure 2B; supplementary material, Table S2). Among the AR-null organoids, those with genomic alterations of *RB1* tended to be less sensitive to treatment compared with 224R-Cx, which does not have any *RB1* alterations (see supplementary material, Figure S5B). This is consistent with a previous study linking *RB1* loss to a decreased response to BET inhibitors [36].

Most studies of BET and CBP/p300 inhibitors have focused on AR-positive models of prostate cancer. To examine AR-null models in more detail, we determined dose responses to NEO2734 compared with JQ1, a representative BET inhibitor, and CPI-637, a representative CBP/p300 inhibitor, using the PrestoBlue cell viability assay. The dose- and time-dependent decreases in

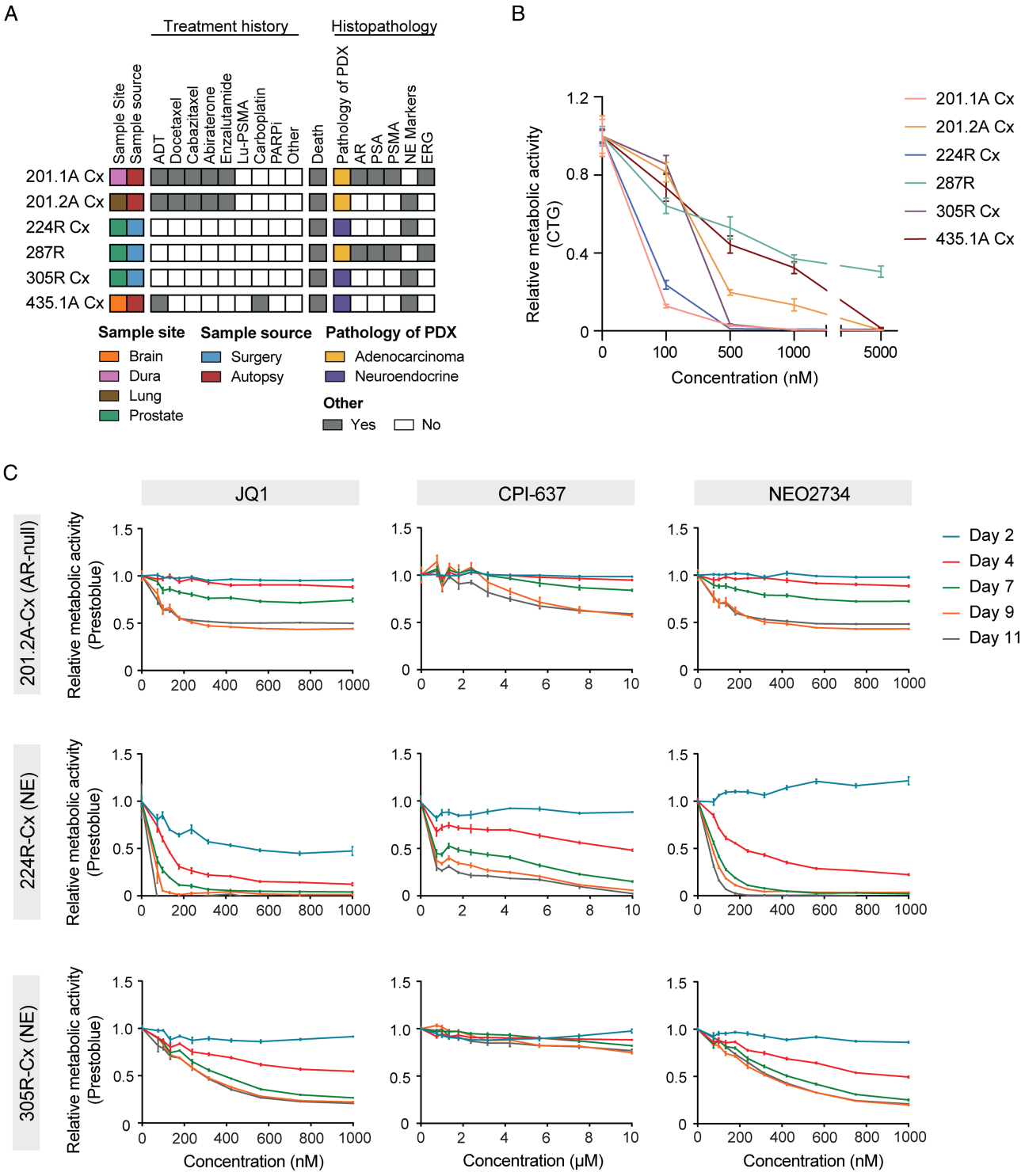

Figure 2. NEO2734 suppresses the growth of AR-positive and AR-null CRPC organoids. (A) Heatmap summarising the features of the six organoids. The data include the site of the original tumour, the source of the tissue, systemic therapies administered to patients prior to sample collection, and follow-up (death). (B) Relative metabolic activity, as measured by CTG, in 201.1A-Cx (red), 201.2A-Cx (yellow), 224R-Cx (blue), 287R (green), 305R-Cx (purple), and 435.1A-Cx (brown) organoids with increasing doses of NEO2734 ($n = 5$ wells). (C) Relative metabolic activity, determined by PrestoBlue viability assay, in organoids established from PDXs 201.2A-Cx (top row), 224R-Cx (middle row), and 305R-Cx (bottom row) on days 2, 4, 7, 9, and 11 treated with vehicle control or increasing concentrations of JQ1, CPI-637, and NEO2734 ($n = 3$). ADT, androgen deprivation therapy; NE, neuroendocrine; PARPi, poly (ADP-ribose) polymerase inhibitor; PSA, prostate-specific antigen; PSMA, prostate-specific membrane antigen.

AR-null organoid viability with NEO2734 treatment were consistent with the previous experiments, with 224R-Cx being the most sensitive AR-null organoid (Figure 2C). Each organoid had a similar response to JQ1 compared with NEO2734, but the responses to CPI-637 were more modest, suggesting that BET inhibition is central to the activity of NEO2734 in these AR-null models. These results confirm the sensitivity of AR-null organoids to NEO2734 and BET inhibition.

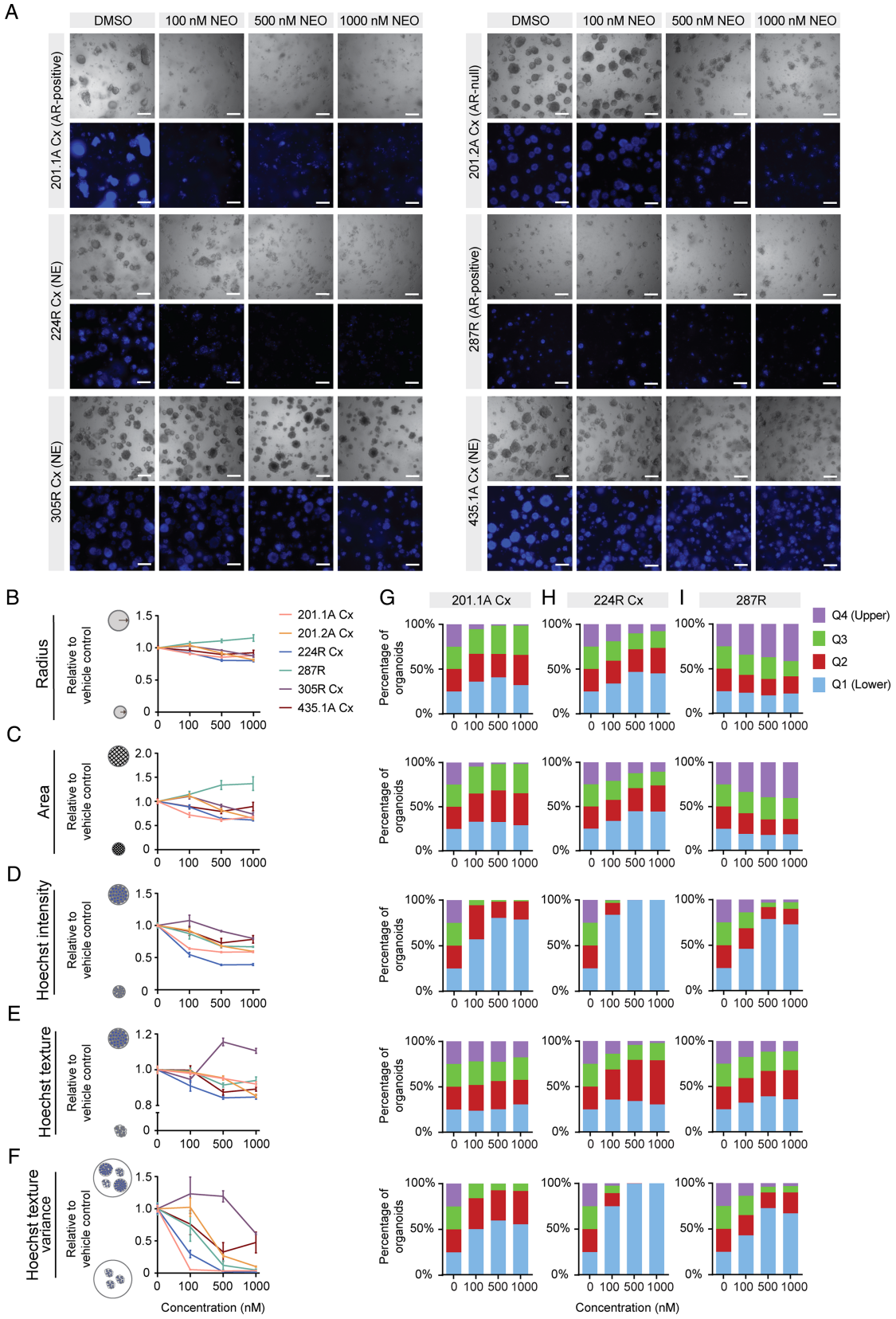

Figure 3. Comparison of organoid responses to NEO2734 across multiple, independent imaging readouts of brightfield microscopy and Hoechst staining. (A) Representative images of brightfield microscopy and Hoechst staining of 201.1A-Cx, 201.2A-Cx, 224R-Cx, 287R, 305R-Cx, and 435.1A-Cx organoids treated for 12 days with vehicle or increasing doses of NEO2734. Scale bars, 100 µm. (B–F) Dose response curves of organoids generated from well-level averages of (B) radius, (C) area, (D) Hoechst intensity, (E) texture, and (F) texture variance treated with increasing doses of NEO2734. Dose–response curves for each tumour treated with NEO2734 were normalised to their respective negative control (DMSO) ($n = 5$ wells). (G–I) For each specific parameter, organoids from each PDX were segregated into quartiles based on the distribution in vehicle control-treated wells. Stacked bar graphs show the percentage of (G) 201.1A-Cx, (H) 224R-Cx, and (I) 287R organoids in each quartile treated with increasing doses of NEO2734. NE, neuroendocrine.

NEO2734 disrupts the size and composition of prostate cancer organoids

Most studies with prostate cancer organoids are limited to bulk measurements of cell viability; however, this does not capture the complexity within and between organoid cultures. Therefore, we performed image analysis of brightfield and fluorescent microscopy of organoids to provide independent readouts of changes in their size and composition (Figure 3A). We focused on five robust measurements of organoid responses to drug treatment [37]. As organoid cultures contain heterogeneous clusters of cells, we accompanied well-based averages of each readout with single organoid analyses (Figure 3B–F). To do this, we segregated individual organoids in each treatment group into quartiles based on the distribution of organoids in the vehicle control-treated wells (Figure 3G–I; supplementary material, Figure S6A–C).

The radius and the area are both measures of organoid size. Consistent with the decreased organoid viability measured with CTG, NEO2734 treatment reduced the average radius and area of all organoids, except 287R (Figure 3B,C; supplementary material, Table S1). Accordingly, single organoid analysis showed that compared with the vehicle control, there was a dose-dependent increase in the proportion of organoids with a small radius and area (blue and red bars) with increasing doses of NEO2734, especially in 201.1A-Cx and 224R-Cx (Figure 3G,H; supplementary material, Figure S6A–C). Additionally, there were fewer organoids with a large radius and area (green and purple bars) with NEO2734 treatment (Figure 3G,H; supplementary material, Figure S6A–C). In contrast, NEO2734 treatment decreased the proportion of small organoids in 287R (Figure 3I). For the remaining tumours, there was still a subset of large organoids after treatment (green and purple bars; supplementary material, Figure S6A–C), but subsequent readouts of organoid composition suggest that these clusters had disintegrated with NEO2734 treatment.

Organoids are multicellular structures. Therefore, we stained DNA with Hoechst and used fluorescence microscopy to measure changes in the cellular composition of organoids using three Hoechst-based readouts as indicators of cell viability. Hoechst intensity, a measure of organoid density, and Hoechst texture, a measure of the degree of uniformity in the composition of each organoid cluster, were decreased in 6/6 and 5/6 organoid cultures, respectively, following NEO2734 treatment (Figure 3D,E,G–I; supplementary material, Figure S6A–C and Table S1), indicating that organoids were sparser with more variable composition following NEO2734 treatment. An exception was 305R-Cx organoids, which showed a higher proportion of organoids with higher Hoechst texture values, suggesting they were more uniform after treatment (Figure 3E; supplementary material, Figure S6B). Lastly, Hoechst texture variance, a measure of intensity variations between different clusters, decreased with NEO2734 treatment in all organoids (Figure 3F–I; supplementary material, Figure S6A–C and Table S1). Thus, NEO2734 treatment reduced the heterogeneity in the composition of organoid cultures, typically resulting in smaller, less-dense clusters containing more variably arranged cells.

Overall, the five readouts of organoid size and composition verified the relative sensitivity of the cultures to NEO2734 treatment. Consistent with the CTG data, 201.1A-Cx and 224R-Cx had the greatest responses to NEO2734 in most readouts. Among the other organoids, 287R and 305R-Cx had different responses to NEO2734 treatment in some parameters, with an increase in size and Hoechst texture following NEO2734 treatment. This was unexpected, so we investigated whether these distinctive phenotypic changes are typical of how these organoids respond to treatment by treating 287R and 305R-Cx organoids with a high dose of docetaxel. Consistent with their response to NEO2734, 287R organoids also increased in radius and area (see supplementary material, Figure S6D), whereas 305R-Cx organoids increased in Hoechst texture (see supplementary material, Figure S6E). Hence, these two organoids have similar responses to docetaxel and NEO2734 across all readouts of organoid viability (see supplementary material, Figure S6F). Therefore, across multiple readouts of viability, size, and composition, AR-positive and AR-null prostate cancer organoids respond to NEO2734.

NEO2734 induces consistent transcriptional responses across organoids

Next, we examined the transcriptional changes in all six organoids after acute 48 h treatment with NEO2734. There were striking changes in mRNA abundance, with 850–3,407 significantly differentially expressed genes in each organoid (false discovery rate [FDR] < 0.05; see supplementary material, Figure S7A). Across all six organoids, 2,348 genes were upregulated and 2,600 were downregulated by NEO2734 (FDR < 0.05; Figure 4A). Previous studies have shown that BET and CBP/p300 inhibitors repress *MYC* [16,38–40] and it was downregulated in three of six organoids (see supplementary material, Figure S7B). Similarly, AR target genes are repressed by BET and CBP/p300 inhibitors [14,17] and we observed that prostatic kallikrein genes were significantly downregulated in the castrate-sensitive organoids (287R), but not the AR-positive castration-resistant organoids (201.1A-Cx) (see supplementary material, Figure S7C).

Each organoid had a distinct set of differentially expressed genes, but there were common transcriptomic differences with NEO2734 treatment across all pairs of organoids (see supplementary material, Figure S7D). Indeed, 22 genes were significantly upregulated and 20 genes were downregulated by NEO2734 in every organoid, regardless of phenotype (Figure 4B; supplementary material, Table S3). The repressed genes included several anti-apoptotic (*ANP32B* and *CLN3*) [41–43] and pro-proliferative factors (*HDGF* and *PHF19L*) [44,45] that are overexpressed in prostate cancer. We also observed

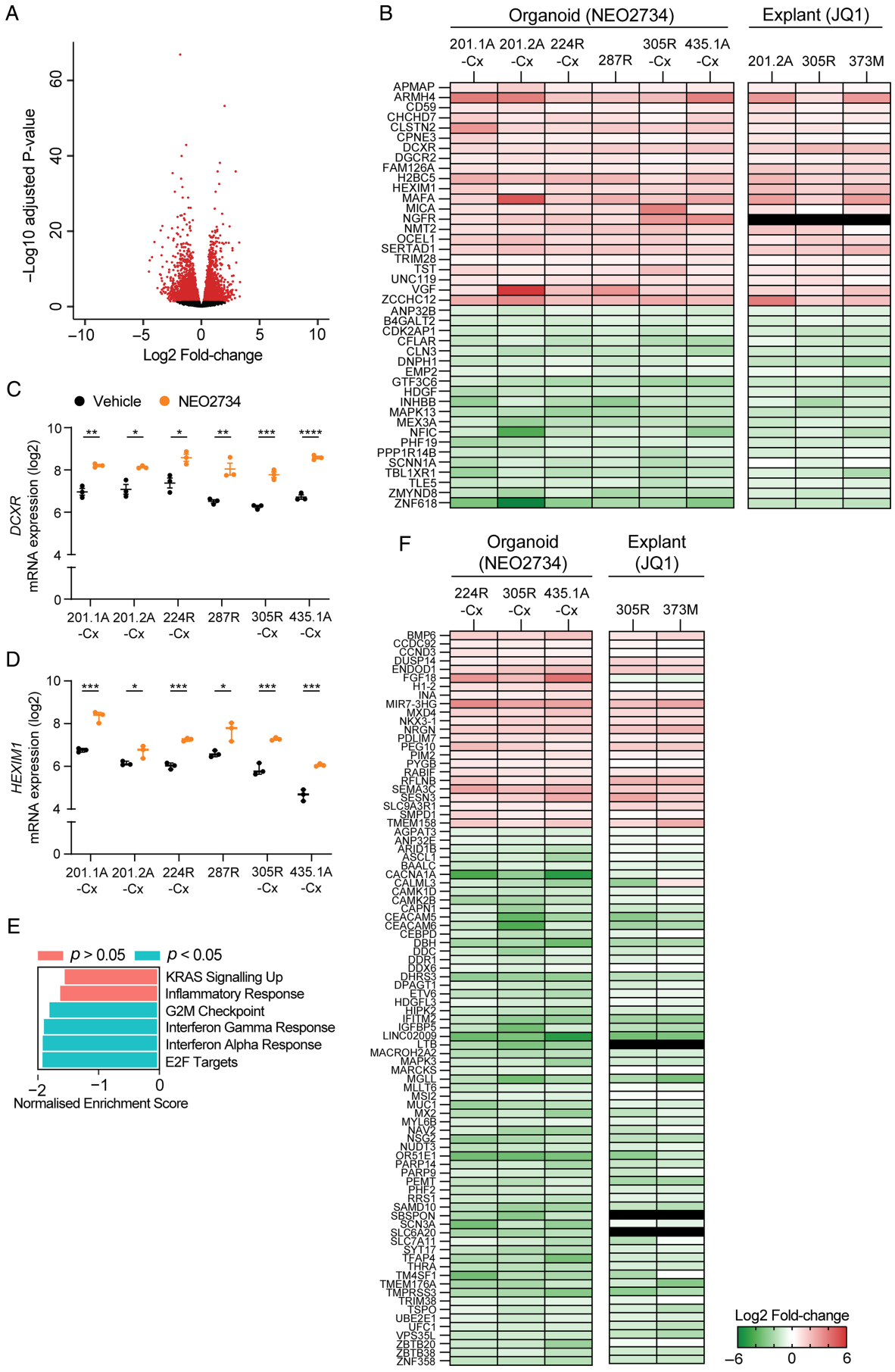

Figure 4 Legend on next page.

decreased *ZMYND8* and *NFIC* expression and increased *DCXR* (Figure 4C) and *HEXIM1* (Figure 4D) expression in every organoid, consistent with previous studies investigating biomarkers of BET inhibitor response in prostate cancer [46,47]. Notably, recent trials of BET inhibitors in prostate cancer patients reported increased *DCXR* and *HEXIM1* expression as reliable indicators of target engagement [48,49]. This reinforces the efficacy of NEO2734 across diverse organoids partly through BET inhibition.

To investigate pathways altered by NEO2734 treatment, we performed GSEA of the hallmark signatures from the Molecular Signatures Database (MSigDB) [50]. There was significantly decreased enrichment of gene sets for activation of E2F transcription factors and cell cycle control after NEO2734 treatment (Figure 4E). There was also a significant reduction in IFN-α and -γ responses, which we interpreted as changes in cell stress based on the gene sets that these hallmark signatures encompass [51]. This is consistent with decreased proliferation with NEO2734 and a previous study showing that BET inhibition blocks E2F1 function in prostate cancer [18].

NEO2734 treatment represses the expression of neuroendocrine markers

The transcriptional responses of NEPC to BET and CBP/p300 inhibitors are poorly understood. To investigate whether NEO2734 induced specific transcriptional changes in NEPC, we identified genes that were only significantly differentially expressed in organoids from neuroendocrine tumours (224R-Cx, 305R-Cx, and 435.1A-Cx) and not in organoids with AR-positive or double-negative pathologies (201.1A-Cx, 201.2A-Cx, and 287R). Across the NEPC organoids, 86 genes were consistently differentially expressed after NEO2734 treatment (23 genes upregulated, 63 genes downregulated) (Figure 4F; supplementary material, Table S4), including downregulation of *CEACAM5* and *TM4SF1*, which are overexpressed in AR-null and NEPC (Figure 4F) [52–54]. There was also decreased expression of *ASCL1*, an important regulator of lineage plasticity and the neuroendocrine phenotype of prostate cancer and small cell lung cancer (Figure 4F) [5,55–57]. We also observed decreased expression of multiple ASCL1 putative target genes, including *CACNA1A, CEACAM5, HIPK2, IGFBP5*, and *SCN3A* [58–60].

The genes that were consistently upregulated by NEO2734 treatment in NEPC organoids included *NKX3.1*, a marker of prostate luminal epithelial cells that regulates differentiation and acts as a tumour suppressor [61]. However, *NKX3.1* transcript counts in NEO2734-treated NEPC organoids were still low compared with baseline levels in the AR-positive organoids. Apart from *NKX3.1*, there was no change in other AR targets and luminal markers, probably because the *AR* was not re-expressed. Similarly, GSEA of AR and neuroendocrine signatures showed no significant changes in NEO2734-treated NEPC organoids at this timepoint (see supplementary material, Figure S7E). Overall, these analyses demonstrate that acute NEO2734 treatment modulates a core set of transcriptional changes in NEPC, including genes associated with the neuroendocrine phenotype.

BET inhibition with JQ1 induces consistent transcriptomic changes in explants

To validate the transcriptional responses of organoids with a different compound and independent set of samples, we treated explants of PDX tissue with JQ1. Slices of tissue from three PDXs (double-negative: 201.2A; NEPC: 305R, 373M) were placed onto gelatin sponges and treated for 48 h with 1 μM JQ1 or vehicle control. The core set of differentially expressed genes from NEO2734-treated organoids was largely concordant in JQ1-treated explants (Figure 4B; supplementary material, Table S3). The trends were also consistent between differentially expressed genes in NEPC organoids and explants (Figure 4F; supplementary material, Table S3). Hence, BET inhibition with NEO2734 or JQ1 induces common transcriptomic changes across different models.

NEO2734 inhibits tumour growth and neuroendocrine signalling of PDXs

As NEO2734 inhibits the growth of prostate cancer cells *in vitro*, we investigated whether it also inhibited tumour growth *in vivo*. We screened the responses of two CRPC PDXs with neuroendocrine pathology, 224R-Cx and 435.1A-Cx, to NEO2734 using the one animal per model per treatment approach (1 × 1 × 1) [33,62]. Based on predefined thresholds for treatment responses [22], 224R-Cx and 435.1A-Cx both had partial responses to NEO2734 with decreased tumour volume after 4 weeks of treatment compared with the vehicle control (Figure 5A). Body weights of mice treated with NEO2734 remained within the ethics criteria (see supplementary material, Figure S7F).

Figure 4. NEO2734 induces consistent transcriptional responses across organoids. (A) Volcano plot of differentially expressed genes (red) identified between untreated and NEO2734-treated organoids (24 h; 1 μM) based on FDR < 0.05 cut-off (black). (B) Heatmap depicting log2 fold-change values for genes that were significantly upregulated (red) and downregulated (green) by NEO2734 in six organoids and JQ1 in three explants. (C and D) Graphs of (C) *DCXR* and (D) *HEXIM1* mRNA expression (log2) in untreated and NEO2734-treated organoids from six PDXs. *$p < 0.05$, **$p < 0.01$, ***$p < 0.001$, ****$p < 0.0001$; unpaired *t*-test ($n = 3$ wells). (E) Top six downregulated pathways across six organoids treated with NEO2734, as determined by the MSigDB enrichment tool (blue bars, $p < 0.05$; red bars, $p > 0.05$). (F) Heatmap depicting log2 fold-change values for genes that were significantly upregulated (red) and downregulated (green) by NEO2734 in three neuroendocrine organoids and JQ1 in two neuroendocrine explants.

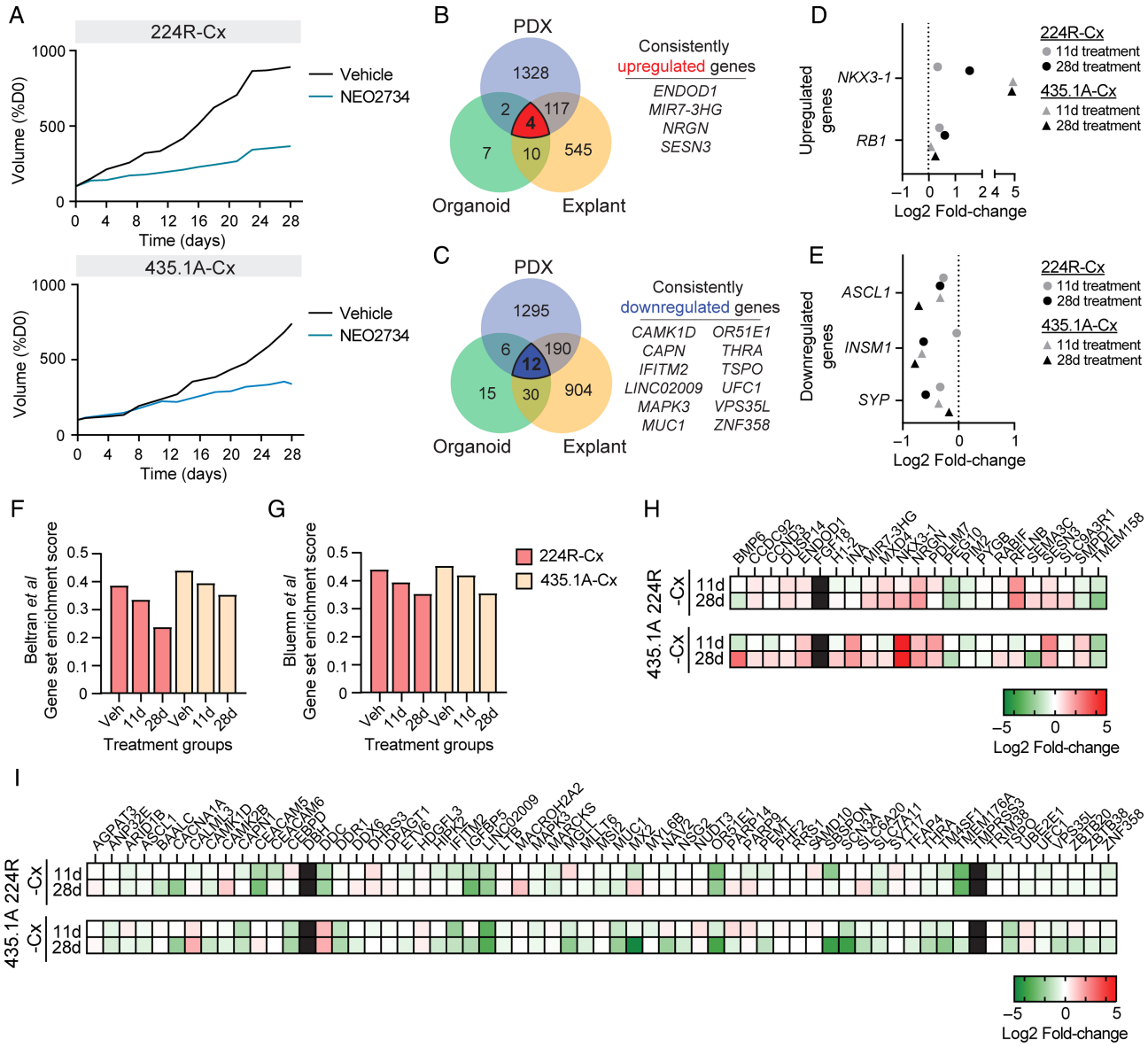

Figure 5. NEO2734 inhibits tumour growth and neuroendocrine signalling in PDXs. (A) Percentage change in tumour volume of PDXs 224R-Cx and 435.1A-Cx treated with vehicle control (black) or NEO2734 (blue) using the one animal per model per treatment (1 × 1 × 1) approach for up to 28 days. (B, C) Venn diagrams showing the overlapping genes that were (B) upregulated and (C) downregulated in JQ1-treated neuroendocrine explants and NEO2734-treated neuroendocrine PDXs at 11 and 28 days, and organoids. Genes consistently upregulated (red) and downregulated (blue) are listed. (D and E) Graphs depicting log2 fold-change of (D) upregulated genes, *NKX3-1* and *RB1*, and (E) downregulated genes, *ASCL1*, *INSM1*, and *SYP* in PDXs 224R-Cx and 435.1A-Cx treated after 11 and 28 days. (F and G) Graphs depicting the (F) Beltran *et al* [3] and (G) Bluemn *et al* [4] gene set enrichment score in PDXs 224R-Cx and 435.1A-Cx treated with vehicle or NEO2734 for 11 and 28 days. (H and I) Heatmaps depicting log2 fold-change values for genes that were significantly (H) upregulated (red) and (I) downregulated (green) by NEO2734 in PDXs 224R-Cx and 435.1A-Cx treated with NEO2734 for 11 and 28 days.

To investigate transcriptional changes associated with tumour growth inhibition following NEO2734 treatment, we performed bulk RNA-sequencing on PDXs 224R-Cx and 435.1A-Cx treated for 11 and 28 days. Across both PDXs, 1,451 genes were upregulated and 1,503 genes were downregulated by NEO2734 treatment at both timepoints (Figure 5B,C). Consistent with the NEPC organoids and explants, *NKX3-1* was upregulated in NEO2734-treated PDXs. NEO2734 also upregulated *RB1*, which frequently undergoes genomic deletions and mutations in NEPC (Figure 5D) [3]. In contrast, NEO2734 repressed several neuroendocrine markers, including *ASCL1*, *INSM1*, and *SYP* (Figure 5E) [63,64]. GSEA showed that NEO2734 treatment suppressed neuroendocrine signatures in both PDXs (Figure 5F,G). There was no evidence of transition to an adenocarcinoma phenotype as there was no increase in the expression of markers of prostate luminal epithelial cells (*AR*, *KLK3*, *FOLH1*, *FOXA1*) and no consistent increase in enrichment of AR signatures (data not shown).

We also compared the transcriptional changes induced by acute *in vitro* and *ex vivo* treatments of organoids and explants versus extended *in vivo* treatments of PDXs. The pattern of upregulated and downregulated genes was

similar across different timepoints and models, although the fold-changes were more modest in PDXs (Figure 5H,I). Four genes were consistently upregulated (*ENDOD1*, *MIR7-3HG*, *NRGN*, *SESN3*) (Figure 5B) and 12 genes were consistently downregulated (*CAMK1D*, *CAPN1*, *IFITM2*, *LINC02009*, *MAPK3*, *MUC1*, *OR51E1, THRA, TSPO, UFC1, VPS35L, ZNF358*) across every organoid, explant, and PDX of NEPC (Figure 5C). These results are consistent with changes in *SESN3* and *MUC1* expression in small cell lung cancer cells treated with OTX015, a novel BET inhibitor [65]. Additionally, MUC1 is overexpressed in aggressive disease, including NEPC [66–69]. Together, these results demonstrate that NEO2734 not only inhibits the growth of patient-derived models of NEPC, it also downregulates the expression of neuroendocrine transcription factors and signalling pathways.

Discussion

Continuous suppression of the AR leads to the emergence of tumours with AR-dependent and AR-independent mechanisms of treatment resistance. Targeting chromatin remodelling, such as with BET and CBP/p300 inhibition, may represent another therapeutic strategy. Initial studies of BET and CBP/p300 inhibitors attributed their efficacy in part due to the disruption of AR signalling; however, recent preclinical and clinical studies have shown promising results in tumours with low AR activity. This prompted us to investigate the effect of BET and CBP/p300 inhibition across the spectrum of prostate cancer pathologies.

The associations between BRD4, CBP, and p300 expression with AR and neuroendocrine signatures are complex. In previous analyses of patient samples, one study showed that *BRD4* was positively correlated with AR levels and an AR signature, whereas another study observed that *BRD4* was upregulated in NEPC, possibly due to different proportions of AR-null tumours in each dataset [17,18]. In our PDX cohort, which had numerous AR-null models, *BRD4* and *p300* mRNA expression were significantly correlated with neuroendocrine and AR signatures, but in opposite directions. However, BRD4, CBP, and p300 each had overlapping distributions in AR-positive and AR-null tumours at both the mRNA and protein level. Therefore, our data demonstrated that BRD4, CBP, and p300 are all expressed in both AR-positive and AR-null prostate cancer.

We investigated the combined inhibition of BRD4, CBP, and p300 with a single agent, NEO2734. Previous studies have examined NEO2734 in advanced prostate cancer, including SPOP-mutant prostate cancer and enzalutamide-resistant CRPC [70,71]. We examined responses to NEO2734 across aggressive subtypes of prostate cancer, including NEPC. NEO2734 inhibited the growth of diverse tumours *in vitro* across multiple readouts, with some organoids more sensitive than others. Among the AR-null organoids, *RB1* status may be a contributing factor, as previously reported [36].

There was a core set of differentially expressed genes in response to NEO2734 treatment across organoids with diverse pathologies. Another BET inhibitor, JQ1, was sufficient to induce the same transcriptional changes in explants. This common set of differentially expressed genes may be a useful pharmacodynamic signature. It includes *HEXIM1*, a well-characterised biomarker of BET inhibition [46,49]. Upregulation of HEXIM1 slows replication forks upon BET inhibitor treatment [72]. This may have contributed to decreased organoid growth regardless of pathology, which was also associated with de-enrichment of the E2F and G2M signatures [18].

Previous studies in AR-positive prostate cancer have shown that CBP/p300 inhibitors and BET inhibitors reduce AR signalling activity. This occurs through reduced transactivation of the AR or reduced AR occupancy at regulator regions of target genes [11,13,14,17]. Here we examined the transcriptomic changes that were specific to NEPC, where there is no AR expression. NEO2734 and JQ1 treatment downregulated several factors involved in neuroendocrine signalling, including *ASCL1*. This is consistent with *ASCL1* being a direct target of BET inhibition in small cell lung cancer [73]. As knockdown of *ASCL1* suppresses the growth of both NEPC and small cell lung cancer, downregulation of *ASCL*1 by NEO2734 and JQ1 may be an additional mechanism of decreased proliferation. Thus, in both AR-positive prostate cancer and NEPC, CBP/p300 and BET inhibitors disrupt the activity of lineage-related transcription factors, specifically the AR and ASCL1.

NEO2734 treatment did not convert NEPC into an adenocarcinoma phenotype, although there was a modest increase in *NKX3.1* expression. This is not surprising, given the stark epigenomic differences between pathologies and the necessity of several regulatory factors for the phenotype of adenocarcinoma, including FOXA1, HOXB13, and the AR [74,75]. Adenocarcinoma and NEPC are often considered to exist along a spectrum [76]. Although adenocarcinoma can transform into NEPC through the selective pressure of treatment, it is not clear if the reverse can also occur, where drug treatment induces neuroendocrine tumours to revert to adenocarcinoma.

We envisage two scenarios where the ability of BET inhibitors to target neuroendocrine circuits may be useful. First, as shown in this study, BET inhibitors may curtail the growth of neuroendocrine tumours by suppressing proliferation and lineage-related factors, such as ASCL1. Second, in tumours that exhibit lineage plasticity, but have not yet lost the AR and other regulatory factors, BET inhibitor treatment may restrain further transformation to AR-null disease. In both cases, it will be important to establish a therapeutic window in the clinic where BET inhibitors can repress neuroendocrine signalling with manageable side-effects. This has been a challenge in previous trials where BET inhibitors have been poorly tolerated by patients. This is probably due to

the broad expression of BET proteins across different somatic cell types, including fibroblasts and neurons [12]. For example, in three separate phase 1 clinical trials of different BET inhibitors, grade ≥ 3 treatment-related adverse events occurred in 19–53% of patients. This included haematological adverse events, such as thrombocytopaenia (4–18%) and anaemia (0–9%) [20,49,77]. Ongoing trials, including the phase 1 study of NEO2734 (NCT05488548) and phase 2 studies of ZEN-3694 (NCT04471974, NCT04986423) may clarify the tolerability of targeting BET proteins in all patients with CRPC, potentially with varying pathology.

In summary, by using patient-derived models to re-evaluate the activity of BET and CBP/p300 inhibition, we demonstrate that NEPC is sensitive to therapies that target chromatin remodelling and suppress the interlinked processes of neuroendocrine signalling and cell proliferation.

Acknowledgements

We acknowledge the people of the Kulin Nations, on whose land these studies were carried out. We pay our respects to their Elders, past and present. We also acknowledge the members of the Prostate Cancer Research program, the patients, families, and consumers who support our research, and the members of the Melbourne Urological Research Alliance (MURAL). For expert assistance, we thank Andrew Bakshi, David Botros, Ashlee Clark, Georgia Cuffe, Jenna Kraska, Melissa Papargiris, Michelle Richards, Mahsa Rostamian Delavar, Hipacia Werneck Gomes, and Prue O'Hare. Thank you to Francis Giles for providing access to NEO2734. The prostate cancer PDX tissue microarray was provided from the Movember Global Action Plan 1 auspiced by MD Anderson Cancer Centre. This work was supported by the National Health and Medical Research Council, Australia (1138242; 1185616); Department of Health and Human Services acting through the Victorian Cancer Agency (MCRF15023, MCRF18017, MCRF17005); the US Department of Defense through the Prostate Cancer Research Program (GPR W81XWH1810349; opinions, interpretations, conclusions, and recommendations are those of the authors and are not necessarily endorsed by the Department of Defense); the CASS Foundation (7139); the EJ Whitten Foundation; Movember Foundation (Global Action Plan 1); the Peter and Lyndy White Foundation; the Rotary Club of Manningham; and TissuPath Pathology. This research was supported by the CASCADE rapid autopsy program, Monash Biomedicine Discovery Institute Organoid Program, Monash University Histology Platform, Monash University Animal Research Laboratories, Peter MacCallum Centre Molecular Genomics Core, and the NeCTAR Research Cloud, a collaborative Australian research platform supported by the National Collaborative Research Infrastructure Strategy. The Victorian Centre for Functional Genomics (KJS) is funded by the Australian Cancer Research Foundation (ACRF), Phenomics Australia (PA) through funding from the Australian Government's National Collaborative Research Infrastructure Scheme (NCRIS), the Peter MacCallum Cancer Centre Foundation, and the University of Melbourne Research Collaborative Infrastructure Program (MCRIP). Open access publishing facilitated by Monash University, as part of the Wiley - Monash University agreement via the Council of Australian University Librarians.

Author contributions statement

NC, RAT, GPR and MGL had full access to all the data in the study and take full responsibility for the integrity of the data and the accuracy of the data analysis. NC, SK, SR, KJS, RAT, GPR and MGL were responsible for the study concept and design. NC, DA, LT, BN, SH and MGL acquired data. NC, SK, SR, DA and MGL analysed and interpreted data. NC and MGL drafted the manuscript. NC, SK, SR, DA, LT, BN, SH, LHP, DLG, KJS, RAT, GPR and MGL critically revised the manuscript for important intellectual content. NC, SK, SR and MGL performed the statistical analysis. RAT, GPR and MGL obtained funding. KJS, RAT, GPR and MGL supervised the study.

Data availability statement

The data that support the findings of this study are openly available in the database of Genotypes and Phenotypes (dbGaP) at https://www.ncbi.nlm.nih.gov/gap/. The study identification number is phs003369.v2.p1.

References

1. Beltran H, Rickman DS, Park K, *et al*. Molecular characterization of neuroendocrine prostate cancer and identification of new drug targets. *Cancer Discov* 2011; **1:** 487–495.
2. Zaffuto E, Pompe R, Zanaty M, *et al*. Contemporary incidence and cancer control outcomes of primary neuroendocrine prostate cancer: a SEER database analysis. *Clin Genitourin Cancer* 2017; **15:** e793–e800.
3. Beltran H, Prandi D, Mosquera JM, *et al*. Divergent clonal evolution of castration-resistant neuroendocrine prostate cancer. *Nat Med* 2016; **22:** 298–305.
4. Bluemn EG, Coleman IM, Lucas JM, *et al*. Androgen receptor pathway-independent prostate cancer is sustained through FGF Signaling. *Cancer Cell* 2017; **32:** 474–489.e6.
5. Nouruzi S, Ganguli D, Tabrizian N, *et al*. ASCL1 activates neuronal stem cell-like lineage programming through remodeling of the chromatin landscape in prostate cancer. *Nat Commun* 2022; **13:** 2282.
6. Park JW, Lee JK, Witte ON, *et al*. FOXA2 is a sensitive and specific marker for small cell neuroendocrine carcinoma of the prostate. *Mod Pathol* 2017; **30:** 1262–1272.
7. Bishop JL, Thaper D, Vahid S, *et al*. The master neural transcription factor BRN2 is an androgen receptor-suppressed driver of neuroendocrine differentiation in prostate cancer. *Cancer Discov* 2017; **7:** 54–71.

8. Hong H, Kao C, Jeng MH, *et al*. Aberrant expression of CARM1, a transcriptional coactivator of androgen receptor, in the development of prostate carcinoma and androgen-independent status. *Cancer* 2004; **101:** 83–89.
9. Tang F, Xu D, Wang S, *et al*. Chromatin profiles classify castration-resistant prostate cancers suggesting therapeutic targets. *Science* 2022; **376:** eabe1505.
10. Thompson D, Choo N, Bolton DM, *et al*. New approaches to targeting epigenetic regulation in prostate cancer. *Curr Opin Urol* 2022; **32:** 472–480.
11. Lasko LM, Jakob CG, Edalji RP, *et al*. Discovery of a selective catalytic p300/CBP inhibitor that targets lineage-specific tumours. *Nature* 2017; **550:** 128–132.
12. Donati B, Lorenzini E, Ciarrocchi A. BRD4 and cancer: going beyond transcriptional regulation. *Mol Cancer* 2018; **17:** 164.
13. Welti J, Sharp A, Yuan W, *et al*. Targeting bromodomain and extra-terminal (BET) family proteins in castration-resistant prostate cancer (CRPC). *Clin Cancer Res* 2018; **24:** 3149–3162.
14. Welti J, Sharp A, Brooks N, *et al*. Targeting the p300/CBP Axis in lethal prostate cancer. *Cancer Discov* 2021; **11:** 1118–1137.
15. Coleman DJ, Gao L, Schwartzman J, *et al*. Maintenance of MYC expression promotes de novo resistance to BET bromodomain inhibition in castration-resistant prostate cancer. *Sci Rep* 2019; **9:** 3823.
16. Wyce A, Degenhardt Y, Bai Y, *et al*. Inhibition of BET bromodomain proteins as a therapeutic approach in prostate cancer. *Oncotarget* 2013; **4:** 2419–2429.
17. Asangani IA, Dommeti VL, Wang X, *et al*. Therapeutic targeting of BET bromodomain proteins in castration-resistant prostate cancer. *Nature* 2014; **510:** 278–282.
18. Kim DH, Sun D, Storck WK, *et al*. BET bromodomain inhibition blocks an AR-repressed, E2F1-activated treatment-emergent neuroendocrine prostate cancer lineage plasticity program. *Clin Cancer Res* 2021; **27:** 4923–4936.
19. Coleman DJ, Gao L, King CJ, *et al*. BET bromodomain inhibition blocks the function of a critical AR-independent master regulator network in lethal prostate cancer. *Oncogene* 2019; **38:** 5658–5669.
20. Aggarwal RR, Schweizer MT, Nanus DM, *et al*. A phase Ib/IIa study of the pan-BET inhibitor ZEN-3694 in combination with enzalutamide in patients with metastatic castration-resistant prostate cancer. *Clin Cancer Res* 2020; **26:** 5338–5347.
21. Spriano F, Gaudio E, Cascione L, *et al*. Antitumor activity of the dual BET and CBP/EP300 inhibitor NEO2734. *Blood Adv* 2020; **4:** 4124–4135.
22. Risbridger GP, Clark AK, Porter LH, *et al*. The MURAL collection of prostate cancer patient-derived xenografts enables discovery through preclinical models of uro-oncology. *Nat Commun* 2021; **12:** 5049.
23. Porter LH, Bakshi A, Pook D, *et al*. Androgen receptor enhancer amplification in matched patient-derived xenografts of primary and castrate-resistant prostate cancer. *J Pathol* 2021; **254:** 121–134.
24. Lawrence MG, Obinata D, Sandhu S, *et al*. Patient-derived models of abiraterone- and enzalutamide-resistant prostate cancer reveal sensitivity to ribosome-directed therapy. *Eur Urol* 2018; **74:** 562–572.
25. Lawrence MG, Porter LH, Choo N, *et al*. CX-5461 sensitizes DNA damage repair-proficient castrate-resistant prostate cancer to PARP inhibition. *Mol Cancer Ther* 2021; **20:** 2140–2150.
26. Toivanen R, Frydenberg M, Murphy D, *et al*. A preclinical xenograft model identifies castration-tolerant cancer-repopulating cells in localized prostate tumors. *Sci Transl Med* 2013; **5:** 187ra171.
27. Wang Y, Revelo MP, Sudilovsky D, *et al*. Development and characterization of efficient xenograft models for benign and malignant human prostate tissue. *Prostate* 2005; **64:** 149–159.
28. Toivanen R, Berman DM, Wang H, *et al*. Brief report: a bioassay to identify primary human prostate cancer repopulating cells. *Stem Cells* 2011; **29:** 1310–1314.
29. Alsop K, Thorne H, Sandhu S, *et al*. A community-based model of rapid autopsy in end-stage cancer patients. *Nat Biotechnol* 2016; **34:** 1010–1014.
30. Lawrence MG, Pook DW, Wang H, *et al*. Establishment of primary patient-derived xenografts of palliative TURP specimens to study castrate-resistant prostate cancer. *Prostate* 2015; **75:** 1475–1483.
31. Porter LH, Hashimoto K, Lawrence MG, *et al*. Intraductal carcinoma of the prostate can evade androgen deprivation, with emergence of castrate-tolerant cells. *BJU Int* 2018; **121:** 971–978.
32. Risbridger GP, Taylor RA, Clouston D, *et al*. Patient-derived xenografts reveal that intraductal carcinoma of the prostate is a prominent pathology in BRCA2 mutation carriers with prostate cancer and correlates with poor prognosis. *Eur Urol* 2015; **67:** 496–503.
33. Gao H, Korn JM, Ferretti S, *et al*. High-throughput screening using patient-derived tumor xenografts to predict clinical trial drug response. *Nat Med* 2015; **21:** 1318–1325.
34. Navone NM, van Weerden WM, Vessella RL, *et al*. Movember GAP1 PDX project: an international collection of serially transplantable prostate cancer patient-derived xenograft (PDX) models. *Prostate* 2018; **78:** 1262–1282.
35. Ouellet V, Erickson A, Investigators GAPUC, *et al*. The Movember global action plan 1 (GAP1): unique prostate cancer tissue microarray resource. *Cancer Epidemiol Biomarkers Prev* 2022; **31:** 715–727.
36. Ding D, Zheng R, Tian Y, *et al*. Retinoblastoma protein as an intrinsic BRD4 inhibitor modulates small molecule BET inhibitor sensitivity in cancer. *Nat Commun* 2022; **13:** 6311.
37. Choo N, Ramm S, Luu J, *et al*. High-throughput imaging assay for drug screening of 3D prostate cancer organoids. *SLAS Discov* 2021; **26:** 1107–1124.
38. Delmore JE, Issa GC, Lemieux ME, *et al*. BET bromodomain inhibition as a therapeutic strategy to target c-Myc. *Cell* 2011; **146:** 904–917.
39. Zuber J, Shi J, Wang E, *et al*. RNAi screen identifies Brd4 as a therapeutic target in acute myeloid leukaemia. *Nature* 2011; **478:** 524–528.
40. Ogiwara H, Sasaki M, Mitachi T, *et al*. Targeting p300 addiction in CBP-deficient cancers causes synthetic lethality by apoptotic cell death due to abrogation of MYC expression. *Cancer Discov* 2016; **6:** 430–445.
41. Shen SM, Yu Y, Wu YL, *et al*. Downregulation of ANP32B, a novel substrate of caspase-3, enhances caspase-3 activation and apoptosis induction in myeloid leukemic cells. *Carcinogenesis* 2010; **31:** 419–426.
42. Khan AP, Poisson LM, Bhat VB, *et al*. Quantitative proteomic profiling of prostate cancer reveals a role for miR-128 in prostate cancer. *Mol Cell Proteomics* 2010; **9:** 298–312.
43. Rylova SN, Amalfitano A, Persaud-Sawin DA, *et al*. The CLN3 gene is a novel molecular target for cancer drug discovery. *Cancer Res* 2002; **62:** 801–808.
44. Shetty A, Dasari S, Banerjee S, *et al*. Hepatoma-derived growth factor: a survival-related protein in prostate oncogenesis and a potential target for vitamin K2. *Urol Oncol* 2016; **34:** 483.e1–483.e8.
45. Jain P, Ballare C, Blanco E, *et al*. PHF19 mediated regulation of proliferation and invasiveness in prostate cancer cells. *Elife* 2020; **9:** e51373.
46. Lin X, Huang X, Uziel T, *et al*. HEXIM1 as a robust pharmacodynamic marker for monitoring target engagement of BET family bromodomain inhibitors in Tumors and surrogate tissues. *Mol Cancer Ther* 2017; **16:** 388–396.
47. Wang L, Xu M, Kao CY, *et al*. Small molecule JQ1 promotes prostate cancer invasion via BET-independent inactivation of FOXA1. *J Clin Invest* 2020; **130:** 1782–1792.
48. Piha-Paul SA, Sachdev JC, Barve M, *et al*. First-in-human study of Mivebresib (ABBV-075), an Oral pan-inhibitor of bromodomain and

extra terminal proteins, in patients with relapsed/refractory solid Tumors. *Clin Cancer Res* 2019; **25:** 6309–6319.
49. Aggarwal R, Starodub AN, Koh BD, *et al*. Phase Ib study of the BET inhibitor GS-5829 as monotherapy and combined with enzalutamide in patients with metastatic castration-resistant prostate cancer. *Clin Cancer Res* 2022; **28:** 3979–3989.
50. Liberzon A, Birger C, Thorvaldsdóttir H, *et al*. The molecular signatures database (MSigDB) hallmark gene set collection. *Cell Syst* 2015; **1:** 417–425.
51. Perelli L, Carbone F, Zhang L, *et al*. Interferon signaling promotes tolerance to chromosomal instability during metastatic evolution in renal cancer. *Nat Cancer* 2023; **4:** 984–1000.
52. DeLucia DC, Cardillo TM, Ang L, *et al*. Regulation of CEACAM5 and therapeutic efficacy of an anti-CEACAM5-SN38 antibody-drug conjugate in neuroendocrine prostate cancer. *Clin Cancer Res* 2021; **27:** 759–774.
53. Lee JK, Bangayan NJ, Chai T, *et al*. Systemic surfaceome profiling identifies target antigens for immune-based therapy in subtypes of advanced prostate cancer. *Proc Natl Acad Sci U S A* 2018; **115:** E4473–E4482.
54. Allioli N, Vincent S, Vlaeminck-Guillem V, *et al*. TM4SF1, a novel primary androgen receptor target gene over-expressed in human prostate cancer and involved in cell migration. *Prostate* 2011; **71:** 1239–1250.
55. Augustyn A, Borromeo M, Wang T, *et al*. ASCL1 is a lineage oncogene providing therapeutic targets for high-grade neuroendocrine lung cancers. *Proc Natl Acad Sci U S A* 2014; **111:** 14788–14793.
56. Borromeo MD, Savage TK, Kollipara RK, *et al*. ASCL1 and NEUROD1 reveal heterogeneity in pulmonary neuroendocrine tumors and regulate distinct genetic programs. *Cell Rep* 2016; **16:** 1259–1272.
57. Cejas P, Xie Y, Font-Tello A, *et al*. Subtype heterogeneity and epigenetic convergence in neuroendocrine prostate cancer. *Nat Commun* 2021; **12:** 5775.
58. Tsuboyama N, Wang R, Szczepanski AP, *et al*. Therapeutic targeting of BAP1/ASXL3 sub-complex in ASCL1-dependent small cell lung cancer. *Oncogene* 2022; **41:** 2152–2162.
59. Wang XD, Hu R, Ding Q, *et al*. Subtype-specific secretomic characterization of pulmonary neuroendocrine tumor cells. *Nat Commun* 2019; **10:** 3201.
60. Castro DS, Martynoga B, Parras C, *et al*. A novel function of the proneural factor Ascl1 in progenitor proliferation identified by genome-wide characterization of its targets. *Genes Dev* 2011; **25:** 930–945.
61. Gurel B, Ali TZ, Montgomery EA, *et al*. NKX3.1 as a marker of prostatic origin in metastatic tumors. *Am J Surg Pathol* 2010; **34:** 1097–1105.
62. Migliardi G, Sassi F, Torti D, *et al*. Inhibition of MEK and PI3K/mTOR suppresses tumor growth but does not cause tumor regression in patient-derived xenografts of RAS-mutant colorectal carcinomas. *Clin Cancer Res* 2012; **18:** 2515–2525.
63. McHugh KE, Mukhopadhyay S, Doxtader EE, *et al*. INSM1 is a highly specific marker of neuroendocrine differentiation in primary neoplasms of the gastrointestinal tract, appendix, and pancreas. *Am J Clin Pathol* 2020; **153:** 811–820.
64. Wiedenmann B, Franke WW, Kuhn C, *et al*. Synaptophysin: a marker protein for neuroendocrine cells and neoplasms. *Proc Natl Acad Sci U S A* 1986; **83:** 3500–3504.
65. Riveiro ME, Astorgues-Xerri L, Vazquez R, *et al*. OTX015 (MK-8628), a novel BET inhibitor, exhibits antitumor activity in non-small cell and small cell lung cancer models harboring different oncogenic mutations. *Oncotarget* 2016; **7:** 84675–84687.
66. Eminaga O, Wei W, Hawley SJ, *et al*. MUC1 expression by immunohistochemistry is associated with adverse pathologic features in prostate cancer: a multi-institutional study. *PLoS One* 2016; **11:** e0165236.
67. Genitsch V, Zlobec I, Thalmann GN, *et al*. MUC1 is upregulated in advanced prostate cancer and is an independent prognostic factor. *Prostate Cancer Prostatic Dis* 2016; **19:** 242–247.
68. Lin X, Gu Y, Kapoor A, *et al*. Overexpression of MUC1 and genomic alterations in its network associate with prostate cancer progression. *Neoplasia* 2017; **19:** 857–867.
69. Yasumizu Y, Rajabi H, Jin C, *et al*. MUC1-C regulates lineage plasticity driving progression to neuroendocrine prostate cancer. *Nat Commun* 2020; **11:** 338.
70. Yan Y, Ma J, Wang D, *et al*. The novel BET-CBP/p300 dual inhibitor NEO2734 is active in SPOP mutant and wild-type prostate cancer. *EMBO Mol Med* 2019; **11:** e10659.
71. He Y, Wei T, Ye Z, *et al*. A noncanonical AR addiction drives enzalutamide resistance in prostate cancer. *Nat Commun* 2021; **12:** 1521.
72. Bowry A, Piberger AL, Rojas P, *et al*. BET inhibition induces HEXIM1- and RAD51-dependent conflicts between transcription and replication. *Cell Rep* 2018; **25:** 2061–2069.e4.
73. Lenhart R, Kirov S, Desilva H, *et al*. Sensitivity of small cell lung cancer to BET inhibition is mediated by regulation of ASCL1 gene expression. *Mol Cancer Ther* 2015; **14:** 2167–2174.
74. Norris JD, Chang CY, Wittmann BM, *et al*. The homeodomain protein HOXB13 regulates the cellular response to androgens. *Mol Cell* 2009; **36:** 405–416.
75. Sahu B, Laakso M, Ovaska K, *et al*. Dual role of FoxA1 in androgen receptor binding to chromatin, androgen signalling and prostate cancer. *EMBO J* 2011; **30:** 3962–3976.
76. Davies AH, Beltran H, Zoubeidi A. Cellular plasticity and the neuroendocrine phenotype in prostate cancer. *Nat Rev Urol* 2018; **15:** 271–286.
77. Lewin J, Soria JC, Stathis A, *et al*. Phase Ib trial with birabresib, a small-molecule inhibitor of bromodomain and extraterminal proteins, in patients with selected advanced solid tumors. *J Clin Oncol* 2018; **36:** 3007–3014.
78. Lawrence MG, Taylor RA, Toivanen R, *et al*. A preclinical xenograft model of prostate cancer using human tumors. *Nat Protoc* 2013; **8:** 836–848.
79. Detre S, Saclani Jotti G, Dowsett M. A "quickscore" method for immunohistochemical semiquantitation: validation for oestrogen receptor in breast carcinomas. *J Clin Pathol* 1995; **48:** 876–878.
80. Gao D, Vela I, Sboner A, *et al*. Organoid cultures derived from patients with advanced prostate cancer. *Cell* 2014; **159:** 176–187.
81. Beshiri ML, Tice CM, Tran C, *et al*. A PDX/organoid biobank of advanced prostate cancers captures genomic and phenotypic heterogeneity for disease Modeling and therapeutic screening. *Clin Cancer Res* 2018; **24:** 4332–4345.
82. Centenera MM, Raj GV, Knudsen KE, *et al*. Ex vivo culture of human prostate tissue and drug development. *Nat Rev Urol* 2013; **10:** 483–487.

References 78–82 are cited only in the supplementary material.

SUPPLEMENTARY MATERIAL ONLINE

Supplementary materials and methods

Figure S1. Association between mRNA expression of epigenetic proteins and AR and neuroendocrine signatures

Figure S2. Validation of specificity of BRD4, CBP, and p300 antibodies for immunohistochemistry using siRNA knockdown

Figure S3. BRD4, CBP, and p300 protein expression in representative PDXs

Figure S4. BRD4, CBP, and p300 protein expression in independent cohorts of prostate cancer PDXs

Figure S5. *BRD4*, *CBP*, *p300*, *AR*, and *RB1* status of organoids

Figure S6. Viability and phenotypic changes in organoids in response to NEO2734 and docetaxel

Figure S7. Transcriptional changes in organoids after NEO2734 treatment

Table S1. Immunohistochemistry conditions for Leica BOND-MAX™

Table S2. Statistical analysis of CTG and imaging readouts at all NEO2734 doses relative to DMSO controls

Table S3. Log2 fold-change (Log2FC) and FDR values for differentially expressed genes in all organoids and explants

Table S4. Log2 fold-change (Log2FC) and FDR values for differentially expressed genes in neuroendocrine organoids and explants